Quantum theory of an atom laser originating from a Bose-Einstein condensate or a Fermi gas in the presence of gravity

Tobias Kramer[1,2,*] and Mirta Rodríguez[1,3,†]
[1]*Instituto de Física, Universidad Nacional Autónoma de México, México D.F., México*
[2]*Department of Physics, Harvard University, 17 Oxford Street, Cambridge, Massachusetts 02138, USA*
[3]*Clarendon Laboratory, University of Oxford, Parks Road, Oxford OX1 3PU, United Kingdom*
(Received 19 April 2006; published 14 July 2006)

We present a three-dimensional quantum-mechanical theory of radio-frequency-outcoupled atom lasers from trapped atomic gases in the presence of the gravitational force. Predictions for the total outcoupling rate as a function of the radio frequency and for the beam wave function are given. We establish a sum rule for the energy-integrated outcoupling, which leads to a separate determination of the coupling strength between the atoms and radiation field. For a noninteracting Bose-Einstein condensate analytic solutions are derived which are subsequently extended to include the effects of atomic interactions. The interactions enhance interference effects in the beam profile and modify the outcoupling rate of the atom laser. We provide a complete quantum-mechanical solution which is in line with experimental findings and allows us to determine the validity of commonly used approximative methods. We also extend the formalism to a fermionic atom laser and analyze the effect of superfluidity on the outcoupling of atoms.

DOI: 10.1103/PhysRevA.74.013611 PACS number(s): 03.75.Pp, 03.75.Ss, 03.65.Nk

I. INTRODUCTION

The possibility of creating an atom laser analogous to an optical laser was considered immediately after the creation of atomic Bose-Einstein condensates (BEC's). Atom lasers can be operated by continuously extracting small amounts of trapped atoms in a coherent way. Atom lasers provide an important tool to analyze the properties of trapped atoms, and many experimental applications are expected due to their coherence properties [1]. In principle they offer the possibility to monitor the evolution of a BEC without the need to switch off the trapping potential.

The first experimental realization of a BEC output coupler was reported in Ref. [2], where short radio-frequency (rf) pulses changed the hyperfine state of the atoms. The inhomogeneous magnetic trapping field separated the atoms into trapped and outcoupled components. Using a series of rf pulses, a sequence of coherent atom waves was formed.

A series of downward-falling output pulses analogous to a pulsed laser was demonstrated in Ref. [3] using an optical lattice. A BEC was loaded into a vertical standing wave created with laser beams pointing in opposite directions. By lowering the depth of the lattice, phase-coherent atoms from different wells tunneled out of the traps and accelerated in the gravitational field. Similarly, it is possible to release an extended wave packet from a single optically trapped BEC by slowly lowering the trapping potential [4,5].

A well-collimated quasicontinuous atom laser was achieved using a stimulated Raman transition as outcoupling mechanism [6]. The two-frequency Raman process imparts a momentum kick to the extracted atoms, allowing directional output coupling. A sequence of overlapping matter wave packets were extracted from a BEC using repeated Raman pulses. Also the first continuous high-flux Raman atom laser has recently been reported [7].

Using an extremely stable novel magnetic trap, Bloch *et al.* [8] demonstrated a quasicontinuous output coupler for magnetically trapped atoms. A weak rf field induces spin flips between trapped and untrapped hyperfine states. The untrapped atoms fall in the gravitational field, producing a collimated atomic beam whose duration is determined by the condensate size. The possibility of continuous feeding the atomic source was demonstrated in Ref. [9]. By applying two different radio frequencies to the same condensate, the coherent spatial nature of the atom laser beam was shown in Ref. [10]. The temporal coherence of atom lasers was investigated in Ref. [11] and more recently also the second-order temporal correlation function [12].

Since atom lasers generate coherent matter waves in the gravitational field of the Earth, an accurate description of the quantum-mechanical propagation in a linear force field is an important part of a theoretical model of an atom laser [13,14]. One-dimensional models [15] are not sufficient for the characterization of the beam wave function, which requires a fully three-dimensional theory. Previous calculations of atom lasers rely mainly on numerical integration without including interactions [16] or employ semiclassical approximations for the propagation in the presence of gravity and a mean-field potential [17–19].

Recently, radial structures perpendicular to the gravitational field have been observed in atom lasers [18,19]. Similar structures have been predicted for smaller condensates [13,20,21], where they are linked to two-path interference in the presence of a linear force field.

In this paper, we formulate and apply a theory of an atom laser, which employs the full three-dimensional (3D) quantum-mechanical propagator. After some basic definitions in Sec. II we review and extend in Sec. III the analytic solution for the beam profile and the total current in the case of a noninteracting BEC. The analytic solvable model of an

*Electronic address: tobias.kramer@mytum.de
†Electronic address: m.pinilla1@physics.ox.ac.uk

atom laser supplied by an "ideal" BEC forms the basis for the inclusion of mean-field potentials in Sec. IV. There, we derive a quantum-mechanical multiscattering theory for the interacting BEC. We compare the quantum solution to experiments and approximative methods like the Born series and the reflection approximation in order to judge the underlying assumptions and shortcomings of these approximations. The inclusion of a mean-field potential changes the emission rate of an atom laser, but the rate still obeys an important sum rule. The beam profile develops a radial substructure, which can be obtained from our quantum-mechanical model and is in line with experimental observations.

The effect of spatially anisotropic traps is discussed in Sec. V, where we show how one-dimensional and three-dimensional models are related.

In Sec. VI we extend the formalism to the current from higher modes in a harmonic trap. We apply it to a quasi-one-dimensional Fermi gas and discuss the effect of fermionic superfluidity in both the current and outcoupled density profile.

The quantum source formalism provides a consistent framework for all presented calculations. A quantum theory for the beam wave function is of special importance for the coherent quantum control and tailoring of matter waves [1].

II. EMISSION RATE AND THE ATOMIC-BEAM WAVE FUNCTION

The output coupling of magnetically trapped atoms can be understood in terms of a spin flip of the magnetic hyperfine quantum number m_F [8,16] (for ^{87}Rb atoms, the $F=1$ hyperfine level is commonly used). Initially, the atoms in the state $|F=1,m_F=-1\rangle$ are in an eigenstate of the atomic trap Hamiltonian in the presence of a static magnetic field B_z and the gravitational field $F=mg$ ($g\approx 9.81\ \mathrm{ms}^{-2}$) along the z axis

$$H_{\mathrm{trap}}^{m_F=-1}=\frac{\mathbf{p}^2}{2m}+\frac{1}{2}m(\omega_x^2x^2+\omega_y^2y^2+\omega_z^2z^2)\delta_{m_F,-1}+m_Fg_F\mu_B\mathcal{B}_z-Fz. \tag{1}$$

Here, g_F denotes the Landé factor and μ_B the Bohr magneton. The inhomogeneous magnetic field of the atom trap is expanded in second order as a harmonic oscillator potential for the $m_F=-1$ state. The gravitational field merely shifts the origin of this oscillator along the z direction and could be absorbed in the quadratic term. The application of an additional oscillating magnetic field with frequency ν and amplitude $\mathcal{B}'$ adds to Eq. (1) the time-dependent potential $V(t)=-\boldsymbol{\mu}\mathcal{B}'\cos(\nu t)$ which causes transitions of the spin to the magnetic quantum number $m_F=0$ (for simplicity we will not consider the $m_F=1$ state). However, the $|F=1,m_F=0\rangle$ state is no longer an eigenstate of the trapping Hamiltonian, which only supports the $m_F=-1$ state. Instead its evolution is governed by the Hamiltonian

$$H_{\mathrm{grav}}^{m_F=0}=\frac{\mathbf{p}^2}{2m}-Fz, \tag{2}$$

which leads to the propagation away from the trap and the formation of an atom laser beam. In the following we will assume a relatively weak amplitude $\mathcal{B}'$ of the oscillating field, which makes it possible to deplete the ground state of the trap over some time. Since our main interest is the determination of the atom laser wave function and the emission rate as a solution of the Schrödinger equation, we will treat the radio wave as a classical radiation field.

At this point we still have to solve for the time-dependent eigenstates ψ'_{trap} and ψ_{grav} of a coupled system, which have an energy difference of $\Delta E=E_{\mathrm{grav}}-E_{\mathrm{trap}}$ and are coupled via $\gamma=\mu\mathcal{B}'$:

$$(i\hbar\partial_t-H_{\mathrm{grav}})\psi_{\mathrm{grav}}(\mathbf{r},t)=\gamma e^{-i\Delta Et/\hbar}\psi'_{\mathrm{trap}}(\mathbf{r},t), \tag{3}$$

$$(i\hbar\partial_t-H_{\mathrm{trap}})\psi'_{\mathrm{trap}}(\mathbf{r},t)=\gamma e^{+i\Delta Et/\hbar}\psi_{\mathrm{grav}}(\mathbf{r},t). \tag{4}$$

Here, we employed the rotating-wave approximation. We split off the time dependence of the states,

$$\psi_{\mathrm{grav}}(\mathbf{r},t)=e^{-iE_{\mathrm{grav}}t/\hbar}\psi_{\mathrm{grav}}(\mathbf{r}), \tag{5}$$

$$\psi'_{\mathrm{trap}}(\mathbf{r},t)=e^{-iE_{\mathrm{trap}}t/\hbar}\psi'_{\mathrm{trap}}(\mathbf{r}), \tag{6}$$

in order to obtain the stationary equations

$$(E_{\mathrm{grav}}-H_{\mathrm{grav}})\psi_{\mathrm{grav}}(\mathbf{r})=\gamma\psi'_{\mathrm{trap}}(\mathbf{r}), \tag{7}$$

$$(E_{\mathrm{trap}}-H_{\mathrm{trap}})\psi'_{\mathrm{trap}}(\mathbf{r})=\gamma\psi_{\mathrm{grav}}(\mathbf{r}). \tag{8}$$

Now we will use the assumption of a weak coupling in order to replace the state $\psi'_{\mathrm{trap}}(\mathbf{r})$ by an eigenstate of Eq. (1) denoted by $\psi_0(\mathbf{r})$. Thus we break the coupling between the two equations and are left with the evaluation of the stationary Schrödinger equation

$$(E_{\mathrm{grav}}-H_{\mathrm{grav}})\psi_{\mathrm{grav}}(\mathbf{r})=\gamma\psi_0(\mathbf{r}) \tag{9}$$

in the presence of an inhomogeneous source term

$$\sigma(\mathbf{r})=\gamma\psi_0(\mathbf{r}). \tag{10}$$

The time-independent source term is akin to the steady-state solution for the atom laser beam after the damping of transient effects due to the initial switching on. In the following, we restrict the discussion to the stationary case. The inhomogeneous equation is readily solved by using the energy-dependent Green function $G_{\mathrm{grav}}(\mathbf{r},\mathbf{r}';E)$ for H_{grav}. The Green function is the solution of the Schrödinger equation for a point inhomogeneity,

$$(E-H_{\mathrm{grav}})G_{\mathrm{grav}}(\mathbf{r},\mathbf{r}';E)=\delta(\mathbf{r}-\mathbf{r}'), \tag{11}$$

and thus we obtain the wave function emitted from an extended source $\sigma(\mathbf{r})$ by a convolution integral:

$$\psi_{\mathrm{grav}}(\mathbf{r};E)=\int d\mathbf{r}'G_{\mathrm{grav}}(\mathbf{r},\mathbf{r}';E)\sigma(\mathbf{r}'). \tag{12}$$

In the following we will suppress the subscript "grav," since we are always interested in the properties of the atomic

beam. We take the energy E as the difference between the energy of the radiation field $h\nu$ minus the Zeeman splitting between the levels $m_F=-1$ and $m_F=0$:

$$E = h\nu - (E_{\text{grav}} - E_{\text{trap}}). \tag{13}$$

Notice that due to the continuous spectrum of $H_{\text{grav}}^{m_F=0}$, an output coupling is possible for a continuous range of energies. However, for $E \to \pm\infty$ we will see that a sum rule for the energy-integrated outcoupling rate enforces a vanishing outcoupling rate. We now proceed to calculate the total current $J(E)$, which denotes the number of atoms released per second. We do this by defining a current density associated with the wave function (12):

$$\mathbf{j}(\mathbf{r};E) = \frac{\hbar}{m}\,\text{Im}[\psi(\mathbf{r};E)^* \boldsymbol{\nabla}\,\psi(\mathbf{r};E)]. \tag{14}$$

By using Eq. (9) it is straightforward to derive the equation of continuity for this stationary problem:

$$\boldsymbol{\nabla}\cdot\mathbf{j}(\mathbf{r}) = -\frac{2}{\hbar}\,\text{Im}\{\sigma(\mathbf{r})^*\psi(\mathbf{r})\}. \tag{15}$$

As wanted, the inhomogeneity models a constantly emitting particle source. The integration over a surface enclosing the source yields a bilinear expression for the total probability current:

$$J(E) = -\frac{2}{\hbar}\,\text{Im}\left\{\int d\mathbf{r}\int d\mathbf{r}'\,\sigma(\mathbf{r})^* G(\mathbf{r},\mathbf{r}';E)\sigma(\mathbf{r}')\right\}. \tag{16}$$

Using the alternative representation of the Green function [14,22],

$$G(\mathbf{r},\mathbf{r}';E) = \langle\mathbf{r}|P\left(\frac{1}{E-H}\right) - i\pi\delta(E-H)|\mathbf{r}'\rangle, \tag{17}$$

we can rewrite Eq. (16) as [14,23]

$$J(E) = \frac{2\pi}{\hbar}\langle\sigma|\delta(E-H)|\sigma\rangle. \tag{18}$$

The quantity $\langle\mathbf{r}|\delta(E-H)|\mathbf{r}\rangle$ is the local density of states (LDOS) of the Hamiltonian H. For initial states normalized to $\langle\psi_0|\psi_0\rangle=N$ an important sum rule [13] follows from Eq. (18):

$$\int_{-\infty}^{\infty} dE J(E) = \frac{2\pi}{\hbar}\langle\sigma|\sigma\rangle = \frac{2\pi\gamma^2 N}{\hbar}. \tag{19}$$

One consequence of the sum rule is that for any Hamiltonian we can determine the interaction strength by simply summing up the total current at different energies. In Ref. [13] this was used to check the experimental reported coupling strength γ. Also the finite value of the integral in Eq. (19) restricts the output coupling to a specific energy range. In the next sections, we derive analytic expressions for the Green function $G(\mathbf{r},\mathbf{r}';E)$.

It is worth mentioning that the source formalism introduced here is analogous to the first-order perturbation theory in the coupling Hamiltonian used for fermionic rf outcoupling in [24–26].

III. IDEAL ATOM LASER

In this section we discuss an extension of the theory for an ideal atom laser presented in Ref. [13]. The ideal case forms the basis for the inclusion of interactions into the theory in Sec. IV. For the Hamiltonian of the linear force field (2) there exists a closed analytic expression of the Green function [27–29]:

$$G_{\text{grav}}(\mathbf{r},\mathbf{r}';E) = \frac{m}{2\hbar^2}\frac{\text{Ci}(u_+)\text{Ai}'(u_-) - \text{Ci}'(u_+)\text{Ai}(u_-)}{|\mathbf{r}-\mathbf{r}'|}, \tag{20}$$

where

$$u_\pm = -\beta[2E + F(z+z') \pm F|\mathbf{r}-\mathbf{r}'|], \tag{21}$$

$$\beta = [m/(4\hbar^2F^2)]^{1/3}, \tag{22}$$

and $\text{Ci}(x)=\text{Bi}(x)+i\text{Ai}(x)$. The application of this Green function to an ideal atom laser from the ground state of a BEC is discussed in detail in [13] and extended to include vortices in rotating BEC's in [14]. In Sec. IV B of [13], an analytic solution for an atom laser originating from a noninteracting isotropic BEC with N atoms of Gaussian form

$$\sigma(\mathbf{r}) = \gamma\sqrt{N}a^{-3/2}\pi^{-3/4}e^{-r^2/2a^2} \tag{23}$$

is derived. Using the scaled variables

$$(\xi,\upsilon,\zeta) = \beta F(x,y,z), \quad \epsilon = -2\beta E, \quad \alpha = \beta F a, \tag{24}$$

$$\tilde{\zeta} = \zeta + 2\alpha^4, \quad \tilde{\rho}^2 = \xi^2 + \upsilon^2 + \tilde{\zeta}^2, \quad \tilde{\epsilon} = \epsilon + 4\alpha^4, \tag{25}$$

and the special functions defined in [14], Appendix B,

$$\text{Q}_1(\rho,\zeta;\epsilon) = -\frac{1}{2\rho}[\text{Ci}(\epsilon-\zeta-\rho)\text{Ai}'(\epsilon-\zeta+\rho) - \text{Ai}(\epsilon-\zeta+\rho)\text{Ci}'(\epsilon-\zeta-\rho)], \tag{26}$$

$$\text{Q}_1^{\text{near}}(\rho,\zeta;\epsilon) = -\int_0^{2\alpha^2} du\frac{e^{-\rho^2/u - u(\epsilon-\zeta)+u^3/12}}{2\pi^{3/2}u^{3/2}} \tag{27}$$

$$\text{Qi}_1(\epsilon) = [\text{Ai}'(\epsilon)]^2 - \epsilon[\text{Ai}(\epsilon)]^2, \tag{28}$$

one obtains analytical expressions for the total current [[14], Eq. (73)],

$$J_{\text{ideal}}(E) = \frac{8}{\hbar}\beta(\beta F)^3\Lambda(\tilde{\epsilon})^2\text{Qi}_1(\tilde{\epsilon}), \tag{29}$$

and the beam wave function

$$\psi_{\text{ideal}}(\mathbf{r};E) = -4\beta(\beta F)^3\Lambda(\tilde{\epsilon})[\text{Q}_1(\tilde{\rho},\tilde{\zeta};\tilde{\epsilon}) + \text{Q}_1^{\text{near}}(\tilde{\rho},\tilde{\zeta};\tilde{\epsilon})]. \tag{30}$$

In addition to Eq. (72) in Ref. [14], we explicitly add the near-field contribution denoted by Q_1^{near}. For the noninteract-

ing case, this term has no influence on the beam profile outside the condensate region, whereas we have to include it for the interacting model in the next section. In both expressions, the source strength $\Lambda(\tilde{\epsilon})$ is strongly energy and size dependent:

$$\Lambda(\tilde{\epsilon}) = \sqrt{N}\gamma(2\sqrt{\pi}a)^{3/2}e^{2\alpha^2(\tilde{\epsilon}-4\alpha^4/3)}. \tag{31}$$

Let us briefly summarize the main features of the ideal atom laser model (see also Sec. IV D):

(i) As shown in [13], Sec. 3.3, the beam wave function can be mapped back to a virtual tunneling point source, which is closely related to the Green function.

(ii) For small condensates (radius $a < \frac{mFa^4}{2\hbar^2}$ in the direction of the gravitational field—i.e., about 0.5 μm for a Rb BEC), additional modulations in the total current appear and the beam wave function develops an interference structure. The emerging pattern can be explained in terms of two-path interference in the linear force field. A typical sequence of beam profiles for different detuning energies is shown in the top panel of Fig. 1.

(iii) For large condensates (radius $a > \frac{mFa^4}{2\hbar^2}$ in the direction of the gravitational field), the energy dependence of the total current reflects the density distribution of the source. The beam wave function is featureless over the whole energy range and well described by an Gaussian profile [13], bottom panel of Fig. 1.

We are not aware of the experimental observations of atom laser beams from small condensates, although high-quality magnetic microtraps are able to produce the required BEC's [31].

For larger condensates one can derive approximative expressions for the total current. Of special simplicity is the so-called reflection approximation, which was developed in the theory of Franck-Condon factors [32]. It is analogous to the local density approximation commonly used in BEC theory and consists of neglecting the kinetic energy term in the Hamiltonian (2). Now Eq. (18) simplifies to

$$J^{\text{refl}}_{\text{ideal}}(E) = \frac{2\pi}{\hbar}\langle\sigma|\delta(E+Fz)|\sigma\rangle = \frac{2\pi}{\hbar}\int d\mathbf{r}|\sigma(\mathbf{r})|^2\delta(E+Fz). \tag{32}$$

The reflection approximation states that the current is proportional to a slice through the initial density distribution along a plane height $z=E/F$. It is possible to justify this approximation as a limit of the quantum solution [see [13], Eq. (40)]. In principle one can also calculate quantum corrections to Eq. (32) (see [20,23,33,34]), but the resulting (asymptotic) series can diverge for a finite number of terms (see Ref. [33], Sec. VI).

The range of validity is limited by the requirement for a large spatial overlap between the initial wave function and the outgoing wave function in order to average over the oscillations of the Airy function in Eq. (20). If the width of the initial wave function is smaller than the first oscillation period of the Airy function [given by approximately $1/(\beta F)$], the oscillations in the outgoing wave function carry over to the total current (see Sec. V).

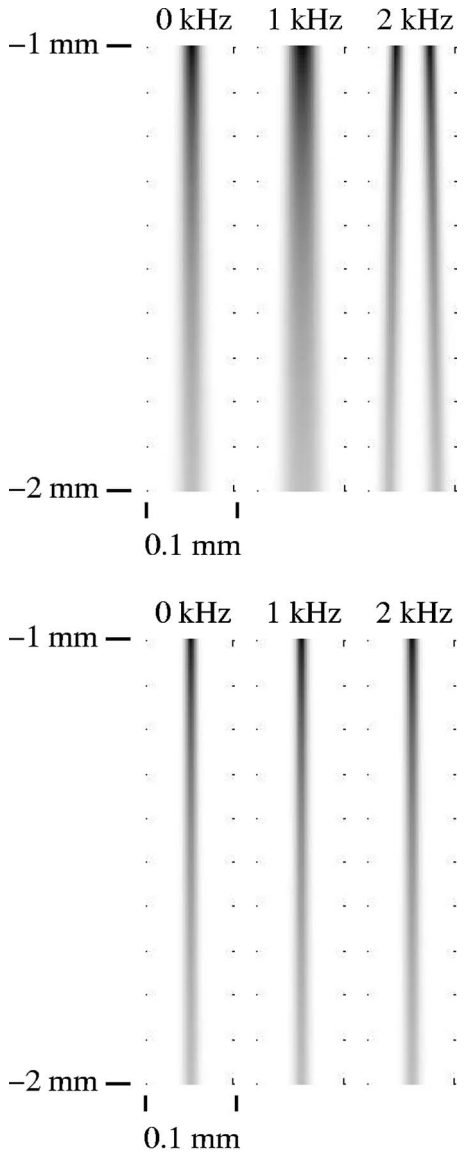

FIG. 1. Atom laser beam profile at different detuning energies $\Delta\nu=E/h$ from Eq. (30) for a relatively small BEC (top panel, $a=0.4$ μm) and a larger BEC (bottom panel, $a=0.8$ μm). For the sign of the detuning see the endnote [30]. Shown is a cut through the middle of the beam along the vertical axis from 1 mm to 2 mm below the BEC for the detuning frequencies (0,1,2) kHz. The beam profile widens and develops a transverse substructure for larger energies. There is rotational symmetry about the vertical-middle axis of each profile. Parameters: $F=m_{\text{Rb}}g$, with $g=9.81$ m/s^2, and $m_{\text{Rb}}=87$ u.

In Fig. 2 we compare the reflection approximation with the quantum-mechanical result Eq. (29).

While the reflection approximation can in certain limits reproduce the total current distribution, it cannot yield information about the atomic beam profile. The slicing picture may be suggestive for the idea that atoms are only outcoupled at the slice given by the condition $z=E/F$. However, this assumption is not supported by the quantum-mechanical result (30). Contrary to the picture of atoms leaving the condensate with zero momentum along a slice [which would in a (semi) classical picture imply that the radial profile of the

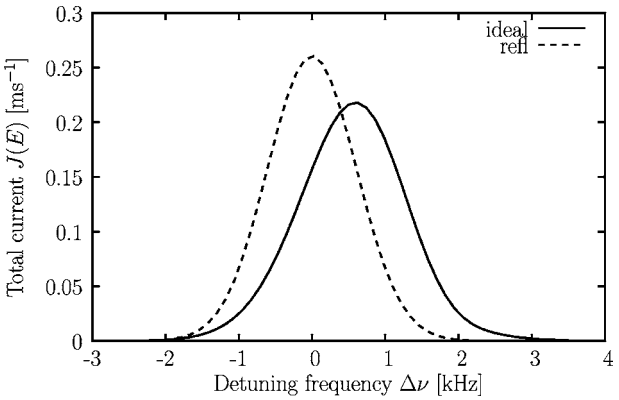

FIG. 2. Total current (per atom) as a function of radio-frequency detuning $\Delta\nu=E/h$ from Eq. (29) (for the sign of the detuning see the endnote [30]). Also shown is the reflection approximation (dashed line). The area underneath the curves is fixed by the sum rule (19). Parameters: $a=0.4$ μm, $\gamma/h=100$ Hz, and $F=m_{\mathrm{Rb}}g$, with $g=9.81$ m/s and $m_{\mathrm{Rb}}=87$ u.

beam at all distances from the BEC is identical to the density profile of the BEC], the beam profile spreads out as shown in Fig. 1. The summation over the infinitely many starting points distributed over the complete BEC is represented by a single point above the center of the condensate, and not by a planar surface at $z=E/F$. The semiclassical picture is further discussed in Sec. IV D.

Simultaneous outcoupling with two different radio frequencies

Experiments which outcouple atom lasers from a BEC with two different radio frequencies at the same time [10] have shown the appearance of longitudinal interference structures. Using the quantum-mechanical theory of the previous section, the resulting atom laser beam is described by the coherent superposition of two stationary beams with different energy originating from the same virtual point source:

$$|\psi_{\mathrm{ideal}}^{\mathrm{two\ rf}}(\mathbf{r},t;\nu_1,\nu_2)|^2=|\psi_{\mathrm{ideal}}(\mathbf{r};h\nu_1)e^{ih\nu_1 t}+\psi_{\mathrm{ideal}}(\mathbf{r};h\nu_2)e^{ih\nu_2 t}|^2. \tag{33}$$

The superposition of the two beam wave functions leads to a time-dependent oscillation of the density profile, which reproduces the observed longitudinal interference structure as shown in Fig. 3. The use of multiple radio frequencies provides an important tool for tailoring the atomic beam wave function.

IV. MEAN-FIELD EFFECTS IN THE ATOM LASER

In this section we extend the quantum theory to include interactions between the BEC and the emitted atom laser beam (interactions within the atomic beam can be neglected since the density is much smaller than inside the BEC). A commonly used approach to include interactions in the description of a BEC is the addition of the (repulsive) mean-field potential via the Gross-Pitaevskii equation [35]

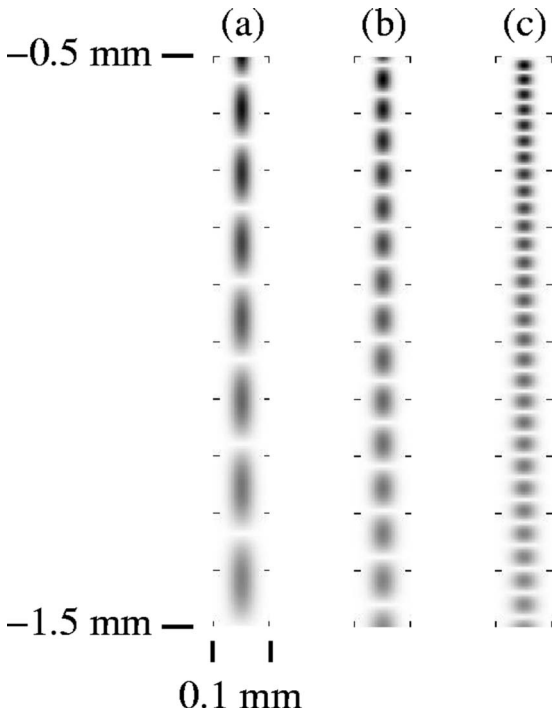

FIG. 3. Squared beam wave function for simultaneous output coupling with two different radio frequencies. Shown is the density given by Eq. (33). The outcoupling frequencies $\Delta\nu_{1,2}$ are (a) ±0.5 kHz, (b) ±1.0 kHz, and (c) ±2.0 kHz. The number of longitudinal interference fringes is proportional to the difference in the detuning frequencies. Parameters: $a=0.8$ μm and $F=m_{\mathrm{Rb}}g$, with $g=9.81$ m/s^2 and $m_{\mathrm{Rb}}=87$ u.

$$V_{\mathrm{GP}}(\mathbf{r})=g_{\mathrm{sc}}|\psi_0(\mathbf{r})|^2, \tag{34}$$

where g_{sc} denotes the interaction strength and is related to the scattering length a_{sc} and the number of atoms in the BEC N via

$$g_{\mathrm{sc}}=4\pi\hbar^2 N a_{\mathrm{sc}}/m. \tag{35}$$

In principle the density-dependent term leads to a nonlinear Schrödinger equation. However, for the theory of the atom laser we will treat the BEC [and $|\psi_0(\mathbf{r})|^2$] as unchanged during the outcoupling process. Therefore we just have to modify the Hamiltonian for the propagating state by the mean-field potential of the BEC:

$$H_{\mathrm{GP}}=\frac{\mathbf{p}^2}{2m}-Fz+g_{\mathrm{sc}}|\psi_0(\mathbf{r})|^2. \tag{36}$$

The additional repulsion will lead to a broadening of the beam compared to the noninteracting case, as we will show next. The repulsive interaction also leads to a change in the BEC density distribution itself. In the following we will retain the Gaussian form of the condensate, but the half-width a of the BEC should be viewed as a parameter, which can be obtained, i.e., by minimizing the Gross-Pitaevskii energy functional [36]. For large condensates, a Thomas-Fermi-like profile of the density is more appropriate than the Gaussian approximation, whereas for condensates in strongly confining traps a Gaussian profile is a fairly good approximation

[31], because larger trapping frequencies increase the ratio of the kinetic energy versus the interaction energy for a constant maximum condensate density (see Ref. [37], Sec. VI B). However, the following discussion and comparison of different methods for the atom laser rate and profile is in principle not limited to an initially Gaussian density distribution.

A. Quantum theory

The Green function of the Hamiltonian (36) is not available in analytic form. In principle, the Born series could be used to construct the Green function

$$G_{\mathrm{GP}} = G_{\mathrm{grav}} + G_{\mathrm{grav}} V_{\mathrm{GP}} G_{\mathrm{grav}} + G_{\mathrm{grav}} V_{\mathrm{GP}} G_{\mathrm{grav}} V_{\mathrm{GP}} G_{\mathrm{grav}} + \cdots . \tag{37}$$

As we will see below, for a typical BEC this series converges very slowly. An alternative approach consists in decomposing the mean-field potential in terms of a δ lattice:

$$V_\delta(\mathbf{r}) = \sum_{j=1}^{N} V_{\mathrm{GP}}(\mathbf{r}_j) \Delta\mathbf{r}\, \delta(\mathbf{r} - \mathbf{r}_j), \tag{38}$$

where $\Delta\mathbf{r}$ denotes the volume element of each lattice site. In order to mimic a continuous potential, the lattice spacing must be smaller than the typical oscillation length of the Green function, which is given by $\lambda \approx 1/(\beta F)$. Numerically, convergence has been checked by a set of calculations with subsequently reduced lattice spacing. For our calculations, we used a spacing of 0.15 μm, which is about $\lambda/4$. The δ lattice is algebraically solvable via the transition (T-)matrix method (for a compact derivation see Ref. [38], Appendix D). The T matrix involves only the known Green function of the linear potential,

$$\mathbf{T}(E)^{-1} = \begin{cases} -G_{\mathrm{grav}}(\mathbf{r}_j, \mathbf{r}_k; E), & j \neq k, \\ [V_{\mathrm{GP}}(\mathbf{r}_j)\Delta\mathbf{r}]^{-1} - G_{\mathrm{grav}}^{\mathrm{norm}}(\mathbf{r}_j, E), & j = k, \end{cases} \tag{39}$$

and the renormalized Green function $G_{\mathrm{grav}}^{\mathrm{norm}}(\mathbf{r};E)$ for $\mathbf{r}=\mathbf{r}'$ [[38], Eq. (D21)]:

$$G_{\mathrm{grav}}^{\mathrm{norm}}(\mathbf{r},E) = \frac{m\beta F}{\hbar^2}[u\mathrm{Ci}(u)\mathrm{Ai}(u) - \mathrm{Ci}'(u)\mathrm{Ai}'(u)], \tag{40}$$

with $u=-2\beta(E+Fz)$. The resulting Green function reads

$$G_{\mathrm{GP}}(\mathbf{r},\mathbf{r}';E) = G_{\mathrm{grav}}(\mathbf{r},\mathbf{r}';E) + \sum_{j,k=1}^{N} G_{\mathrm{grav}}(\mathbf{r},\mathbf{r}_j;E)\mathbf{T}_{jk}(E,\mathbf{r}_j,\mathbf{r}_k)G_{\mathrm{grav}}(\mathbf{r}_k,\mathbf{r}';E). \tag{41}$$

Using the Green function G_{GP}, we proceed to calculate the total current from Eq. (16):

$$\begin{aligned} J_{\mathrm{GP}}(E) &= -\frac{2}{\hbar}\,\mathrm{Im}\Big[\langle\sigma|G_{\mathrm{grav}}|\sigma\rangle + \sum_{j,k}\mathbf{T}_{jk}(E)\psi_{\mathrm{ideal}}(\mathbf{r}_j;E)\psi_{\mathrm{ideal}}(\mathbf{r}_k;E)\Big] \\ &= J_{\mathrm{ideal}}(E) + J_{\mathrm{GP}}^{\delta}(E). \end{aligned} \tag{42}$$

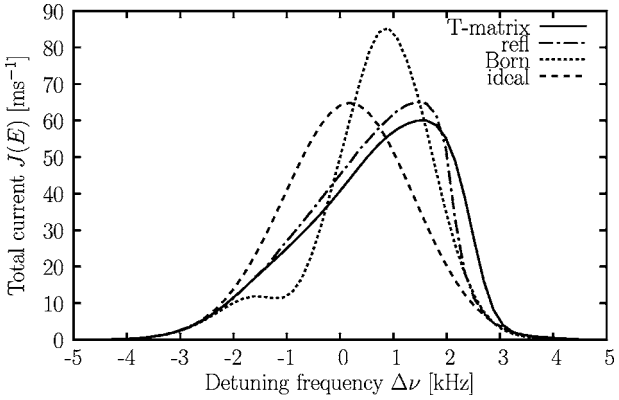

FIG. 4. Total current for a BEC of $N=500$ atoms as a function of the detuning frequency $\Delta\nu = E/(2\pi\hbar)$. We compare the results using the T-matrix method (42) (with 1309 lattice points spaced at distances of 0.15 μm), the reflection approximation (46), the first -order Born approximation (45), and the noninteracting result (29). Parameters: $N=500$ atoms, $a_{\mathrm{scat}}=5.77$ nm, $a=0.8$ μm, $\gamma/h = 100$ Hz, and $F=m_{\mathrm{Rb}}\,g$, with $g=9.81$ m/s^2 and $m_{\mathrm{Rb}}=87$ u.

The sum rule (19) enforces that the changes of the current vanish upon integration over the outcoupling frequency:

$$\int_{-\infty}^{\infty} dE J_{\mathrm{GP}}^{\delta}(E) = 0. \tag{43}$$

Similarly, the beam wave function [see Eq. (12)] is given by the sum of the ideal profile and an interaction term

$$\begin{aligned} \psi_{\mathrm{GP}}(\mathbf{r};E) &= \psi_{\mathrm{ideal}}(\mathbf{r};E) + \sum_{j,k}\ \mathbf{T}_{jk}(E)G_{\mathrm{grav}}(\mathbf{r},\mathbf{r}_j;E)\psi_{\mathrm{ideal}}(\mathbf{r}_k;E)] \\ &= \psi_{\mathrm{ideal}}(\mathbf{r};E) + \psi_{\mathrm{GP}}^{\delta}(\mathbf{r};E). \end{aligned} \tag{44}$$

B. First-order Born and reflection approximation

Within the T-matrix approach, we obtain the first-order Born approximation by setting

$$\mathbf{T}_{jk}^{\mathrm{Born}}(E) = \delta_{jk} V_{\mathrm{GP}}(\mathbf{r}_j)\Delta\mathbf{r}. \tag{45}$$

In general, the first-order approximation is not sufficient for an accurate description, as shown in Fig. 4.

In analogy to the noninteracting case, we can include the mean-field potential in the reflection approximation. The previously planar slices are now distorted, depending on the density of the condensate wave function:

$$J_{\mathrm{GP}}^{\mathrm{refl}}(E) = \frac{2\pi}{\hbar}\int d\mathbf{r}|\sigma(\mathbf{r})|^2\delta(E + Fz - V_{\mathrm{GP}}(\mathbf{r})). \tag{46}$$

C. Comparison of the quantum theory and approximative methods

In Fig. 4 we compare the results of the different methods for the total current as a function of the detuning frequency. We choose a Gaussian condensate with half width $a = 0.8$ μm, for which we expect a tunneling behavior up to detuning energies of $Fz_0 \approx 8$ kHz. The ideal (noninteracting)

total current reflects the Gaussian density profile of the condensate and attains therefore a symmetric shape. The inclusion of the mean-field potential shifts the maximum of the total current to higher energies, as shown by the quantum-mechanical T-matrix calculation. The reflection approximation works surprisingly well, whereas the first-order Born approximation gives a misleading result with an additional hump. Notice that the area underneath all curves is the same, as required by the sum rule (19). The shift to higher values of the detuning frequency in the maximum of the output coupling is in agreement with experimental results reported in [8,16] (note that the definition of the sign of the detuning frequency used here is opposite from the one used in the experimental work).

Due to the effective negative initial kinetic energy, the beam profile of the noninteracting atom laser has a Gaussian profile, without a radial substructure (see [13]). However, the presence of the repulsive mean-field potential affects the beam profile considerably as shown in Fig. 5. In the transverse direction a substructure develops, which has been observed experimentally [18,19]. In a simple one-dimensional picture, the widening of the beam profile as compared to the noninteracting case has been attributed to the repulsive hump in the potential acting as a diverging lens [17]. The three-dimensional quantum-mechanical picture is more involved, since the T-matrix approach includes multiple-scattering events and no simple semiclassical interpretation in terms of trajectories is available.

D. Semiclassical models for the beam profile

The appearance of an interference structure in matter wave experiments can be linked to the possibility of multiple paths from the source (or emitter) of the wave to the location of the detector. In the presence of a linear force field, the classical double-slit experiment for electrons [39] was carried out by Blondel *et al.* [40,41] without actually constructing a material double slit. The uniform field environment provides (for positive initial kinetic energy) a region, in which there are two paths connecting the source with the target [42]. In the semiclassical approximation of the energy Green function all classically allowed paths carry a complex amplitude (determined by the classical action) and are added coherently [14,43–45].

In contrast to the classical analysis of the trajectories from a single point in space to another point, a spatially extended source region, like a BEC, seems to require the addition of infinitely many paths leading from every point of the source region to the target point. Remarkably, the single-point interference pattern is not destroyed by this averaging process. The reason is that, similar to the technique of virtual point sources in optics, one may replace the extended BEC by a single-point source which is located at a distance

$$z_0 = -\frac{mFa^4}{2\hbar^2} = -\frac{g}{2\omega^2} \tag{47}$$

above the center of the BEC [13] [we used $a=\sqrt{\hbar/(m\omega)}$]. The focal point of the parabola given by the trapping potential (converted to spatial units) $V_{\mathrm{trap}}(z)/F=\frac{1}{2F}m\omega^2 z^2$ coincides with the location of the virtual point source at a distance z_0 from the condensate. Due to the shift upwards in the gravitational field, the initially available kinetic energy is reduced by the potential energy at the shifted location

$$E_{\mathrm{kin}} = h\Delta\nu - V_{\mathrm{GP}}(0,0,z_0) - |Fz_0|. \tag{48}$$

Here, we also included the potential term due to the mean field of the condensate atoms, which creates a hump in the otherwise planar potential surface of the linear gravitational

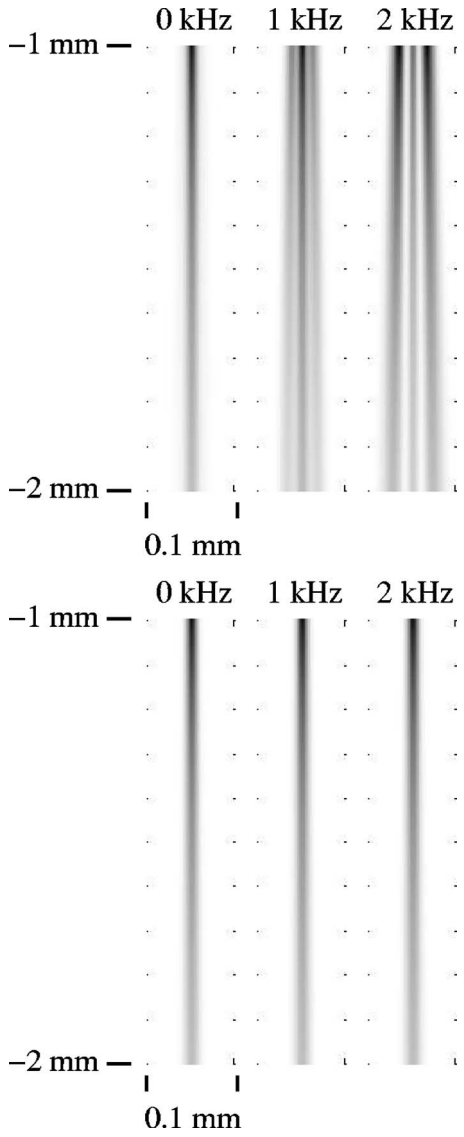

FIG. 5. Top panel: atom laser beam profile from Eq. (44) at different detuning energies $\Delta\nu=E/h$ including interactions ($N=500$ atoms, $a_{\mathrm{scat}}=5.77$ nm), other parameters as in Fig. 4. The beam profile broadens and develops a transverse substructure for larger energies. Bottom panel: atom laser profiles for the same detuning frequencies and condensate width, but without interactions. The transverse interference pattern is not present. For the sign of the detuning see the endnote [30]. Shown is a cut through the middle of the beam along the vertical axis from 1 mm to 2 mm below the BEC for the detuning frequencies (0,1,2) kHz. There is rotational symmetry about the vertical-middle axis of each profile.

field. For a large condensate, the initial shift $|z_0| \gg a$ leads to a virtual point source which is actually located several half widths a apart from the center of the BEC. The resulting initial kinetic energy is negative for detuning energies in the range of energies for which we expect a significant total current $h\Delta\nu < Fa$. For the semiclassical analysis we note that no classical trajectories exist up to the turning surface, which is given by the implicit equation

$$h\Delta\nu - V_{\mathrm{GP}}(0,0,z) - |Fz| = 0. \tag{49}$$

In principle, one can study the classical trajectories which start from this caustic surface and end at a given target point. The possibility of multiple trajectories leads to a coherent sum over the corresponding classical actions [17,19]. However, a caustic surface is not an ideal starting point for a semiclassical analysis, since the specification of an initial position and simultaneously a definite momentum $\mathbf{p}=0$ is not compatible with the uncertainty relation [45]. The unknown initial phase and weight of the manifold of classical trajectories starting from the caustic surface presents another difficulty for a well-defined semiclassical description.

V. GEOMETRY EFFECTS IN THE ATOM LASER

So far we have only considered spherically symmetric clouds of atoms. In principle one can tune the magnetic trapping potential and thus vary the frequencies of the harmonic trap. Experimentally it is possible to obtain quasi-1D systems [46,47] by tuning one of the frequencies of the 3D trap to a value which is much smaller than the other frequencies or by using optical lattices to create arrays of smaller 1D systems [48]. A 1D gas with the long axis in the direction of the gravitational field is characterized by $\omega_z \ll \omega_\perp = (\omega_x^2 + \omega_y^2)^{1/2}$. The propagation occurs in the three-dimensional space, and thus it is not sufficient to consider merely the propagation in the gravitational field along the beam axis. While the total energy is conserved, it falls into parts related to propagation in the direction of the gravitational field and in the perpendicular plane, respectively. In the following we analyze the relationship between three-dimensional and one-dimensional calculations. For simplicity we do not include mean-field effects in the calculations.

We consider the current and outcoupled wave function for an initial state of the form

$$\psi_{\mathrm{ini}}(x,y,z) = \langle \mathbf{r}|\psi_{\mathrm{ini}}\rangle = \psi_0^{\perp}(x,y)\psi_0(z), \tag{50}$$

where $\psi_0(z)$ and $\psi_0^{\perp}(x,y) = 1/\sqrt{\pi a_\perp^2}\, e^{-(x^2+y^2)/2a_\perp^2}$ are the ground states of the harmonic oscillator with half width $a = \sqrt{\hbar/(m\omega_z)}$ and $a_\perp = \sqrt{\hbar/(m\omega_\perp)}$. The connection between the 1D and 3D Green functions of the linear gravitational field is given by a convolution integral over the transverse momenta k and k':

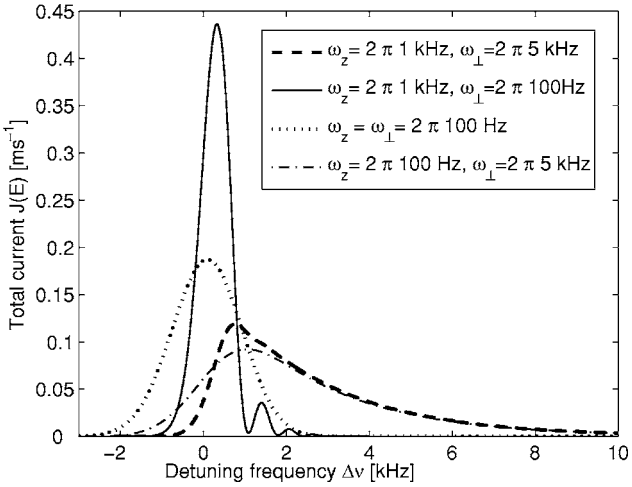

FIG. 6. Total current (per atom) as a function of the detuning frequency $\Delta\nu = E/h$. Shown is the 3D total current (53) for several geometries. Parameters: $\gamma/h = 100$ Hz and $m_{\mathrm{Na}} = 23$ u.

$$G_{\mathrm{grav}}^{\mathrm{3D}}(\mathbf{r},\mathbf{r}';E) = \frac{1}{(2\pi)^2}\int\int dk\, dk'\, e^{-ik(x-x')-ik'(y-y')} G_{\mathrm{grav}}^{\mathrm{1D}} \times \left(z,z';E-\frac{\hbar^2(k^2+k'^2)}{2m}\right), \tag{51}$$

where [[38], Eq. (B2)]

$$G_{\mathrm{grav}}^{\mathrm{1D}}(z,z';E) = -4\pi\beta^2 F \mathrm{Ci}(u_+)\mathrm{Ai}(u_-). \tag{52}$$

For the total current (16) we evaluate the expectation value of the Green function with respect to the initial state ψ_{ini}. The resulting convolution integral reads

$$J^{\mathrm{3D}}(E) = 2a_\perp^2 \int_0^\infty dk_\perp k_\perp e^{-a_\perp^2 k_\perp^2} J^{\mathrm{1D}}\left(E - \frac{\hbar^2 k_\perp^2}{2m}\right), \tag{53}$$

where

$$J^{\mathrm{1D}}(E) = \frac{16\beta\pi^{3/2}\alpha\gamma^2 N}{\hbar} e^{-(16/3)\alpha^6 + 4\alpha^2\tilde{\epsilon}} \mathrm{Ai}(\tilde{\epsilon})^2 \tag{54}$$

is derived in Eq. (65).

In Fig. 6 we show the 3D total currents for a big condensate [$|z_0| > a$ or $Fa > 2\hbar\omega_z$; see Eq. (47)] whose width along the gravitational axis is $a = 2.1$ μm ($\omega_z = 2\pi \times 100$ Hz) and for a small BEC with $a = 0.66$ μm ($\omega_z = 2\pi \times 1$ kHz). Figure 6 shows the current for Na atoms instead of Rb, since then the condition for small condensates is fulfilled for smaller trapping frequencies. In the reflection approximation, Eq. (32), we expect that the outcoupling window is just determined by the condensate extension along the gravitational field and not changed for the one-dimensional and three-dimensional cases.

However, the convolution integral (53) of the 1D current with an exponentially decaying function whose width is proportional to $\omega_\perp$ predicts in general a different form of the 1D and 3D current. This effect can be clearly seen in Fig. 6. Only for a large condensate the 3D current retains a Gaussian

shape (see the dotted line in Fig. 6). A tight confinement in the transverse direction results in a spread of the total current as shown by the dot-dashed line in Fig. 6.

For small condensates the situation changes completely. Now the total current in 1D is modulated by the zeros of the Airy function in Eq. (54). The convolution with the transverse momentum tends to wash out the zeros if $\omega_\perp$ is big enough (dashed line in Fig. 6), but there might still exist regions of almost complete suppression of the total current within the outcoupling energy window (see the solid line in Fig. 6).

One can also separate the expressions for the 1D and 3D outcoupled wave functions. The outgoing wave function perpendicular to the gravitational force is given by

$$\psi_{\text{out}}^{\perp}(x,y) = \frac{1}{4a_\perp \pi^{5/2}} \int\int dk\, dk' \int\int dx'\, dy' \times e^{-ik(x-x')-ik'(y-y')-(x'^2+y'^2)/2a_\perp^2} = \int dk_\perp \frac{a_\perp k_\perp}{\sqrt{\pi}} e^{-a^2k_\perp^2/2} J_0(k_\perp\sqrt{x^2+y^2}), \quad (55)$$

where J_0 denotes the Bessel function of zeroth order. The corresponding 3D wave function reads

$$\psi_{\text{out}}^{\text{3D}}(\mathbf{r};E) = \frac{a_\perp}{\sqrt{\pi}} \int_0^\infty dk_\perp k_\perp e^{-a_\perp^2 k_\perp^2/2} J_0(k_\perp\sqrt{x^2+y^2}) \times \psi_{\text{out}}^{\text{1D}}\left(z;E-\frac{\hbar^2k_\perp^2}{2m}\right), \quad (56)$$

where

$$\psi_{\text{out}}^{\text{1D}}(z;E) = 4\sqrt{2F\alpha N}\gamma\beta^{3/2}\pi^{5/4}e^{-(8/3)\alpha^6+2\alpha^2\tilde{\epsilon}}\text{Ai}(\tilde{\epsilon})\text{Ci}(\tilde{\epsilon}-2\tilde{\xi}). \quad (57)$$

Similar to the total current, the three-dimensional wave function is given by the convolution of the one-dimensional wave function and an exponentially decaying function whose width is proportional to $\omega_\perp$.

VI. CURRENT FROM HIGHER MODES IN A HARMONIC TRAP: FERMIONIC ATOM LASER

In this section we consider the current and outcoupled wave function from excited modes in a harmonic trap. In particular we consider a fermionic gas at $T=0$, but the formalism presented here can also be used to analyze the contribution to the current and outcoupled beam of the higher modes in a trapped BEC.

Quantum degeneracy was demonstrated for a trapped cloud of fermionic alkali atoms in [49]. A gas of ultracold fermionic atoms becomes superfluid [50–54] by tuning the interaction strength between two different hyperfine states. Fermionic superfluidity relies on the formation of pairs of attractive atoms. In the limit of weak interactions the system can be described by the Bardeen-Cooper-Schrieffer (BCS) theory developed in superconductivity that relates the order parameter to the binding energy of the paired atoms (gap). A beam of atoms coherently outcoupled from a trapped gas preserves the properties of the initial state of the atoms. We explore the effect of quantum degeneracy and fermionic superfluidity in the outcoupled beam density profile and the total current. For the sake of simplicity we consider quasi-one-dimensional systems. Furthermore, it is reasonable to expect that the effect of superfluidity in the outcoupling increases when the superfluid gap is highest along the direction of gravity.

A. Excited modes falling in the gravitational field

In this section we present a one-dimensional calculation of an excited state of a harmonic trap falling in the gravitational field. The current is calculated from the Franck-Condon factors of the initial and final eigenfunctions. The initial Hamiltonian of a 1D harmonic oscillator reads

$$H_{\text{trap}}^{\text{1D}} = -\frac{\hbar^2}{2m}\frac{d^2}{dz^2} + \frac{1}{2}m\omega_z^2 z^2, \quad (58)$$

whose eigenstates and eigenenergies are given by

$$\psi_n(z) = \frac{1}{\pi^{1/4}\sqrt{a2^n n!}} H_n\left(\frac{z}{a}\right)\exp\left(-\frac{z^2}{2a_z^2}\right), \quad (59)$$

$$E_n = \hbar\omega_z\left(n+\frac{1}{2}\right), \quad (60)$$

where $a=\sqrt{\hbar/m\omega_z}$. The final-state Hamiltonian is given by the 1D version of H_{grav} defined in Eq. (2):

$$H_{\text{f}} = -\frac{\hbar^2}{2m}\frac{d^2}{dz^2} - Fz. \quad (61)$$

The Hamiltonian H_{f} has a continuous spectrum and the eigenfunctions can be labeled by the energy [55]

$$\psi_E^{\text{f}}(z) = \langle z|\psi_E^{\text{f}}\rangle = 2\sqrt{F}\beta\text{Ai}\left(-2\beta F\left(z+\frac{E}{F}\right)\right). \quad (62)$$

Inserting the complete set of continuum eigenfunctions in Eq. (18) yields the following expression for the total current originating from an initial state $|\psi_n\rangle$:

$$J_n^{\text{1D}}(E) = \frac{2\pi\gamma^2}{\hbar}\int dE_{\text{grav}}\delta(E-E_{\text{grav}})|\langle\psi_n|\psi_E^{\text{f}}\rangle|^2. \quad (63)$$

The needed overlap integrals (which are Franck-Condon factors) are conveniently calculated by adapting a recursive method developed in Ref. [55] (see also Appendix A):

$$\langle\psi_n|\psi_E^{\text{f}}\rangle = \sqrt{\frac{8\sqrt{\pi}\beta\alpha}{2^n n!}}\exp\left(\frac{16\alpha^6}{3}-4\beta E\alpha^2\right) \times K(n,2,-8\alpha^3,-2\beta E+4\alpha^4,-4\alpha). \quad (64)$$

Here, $K(n,\alpha_L,\alpha_L',\gamma_L,\delta_L)$ is given by Eq. (A5). The 1D current becomes

$$J_n^{\text{1D}}(E) = \frac{2\pi\gamma^2}{\hbar}|\langle\psi_n|\psi_E^{\text{f}}\rangle|^2. \quad (65)$$

The outcoupled wave function can be calculated from Eq. (12):

$$\psi_{\text{out}}^{\text{1D}}(n,z;E) = \gamma \int dz' G_{\text{1D}}(z,z';E)\psi_n(z'). \tag{66}$$

As shown in the Appendix, a closed expression is given by Eq. (A4)

$$\psi_{\text{out}}^{\text{1D}}(n,z;E) = B(n,z,E)K(n,2,-8\alpha^3,-2\beta E+4\alpha^4,-4\alpha), \tag{67}$$

where $B(n,z,E)$ is defined in the Appendix.

B. Long axis in the direction of gravity

We consider the current and outcoupled function for an initial state of the form

$$\psi_{\text{ini}}(x,y,z) = \langle \mathbf{r}|\psi_{\text{ini}}\rangle = \psi_0(x)\psi_0(y)\psi_n(z), \tag{68}$$

where ψ_i are the eigenstates of the harmonic oscillator. Thus we consider an arbitrary excited state along the z direction while the wave functions are Gaussians in the perpendicular plane. The total current is given by a convolution integral with the 1D current of Eq. (65):

$$J_n^{\text{3D}}(E) = 2a_\perp^2 \int_0^\infty dk_\perp k_\perp e^{-a_\perp^2 k_\perp^2} J_n^{\text{1D}}\left(E - \frac{\hbar^2 k_\perp^2}{2m}\right). \tag{69}$$

The corresponding 3D outcoupled wave function is obtained by using Eq. (56):

$$\psi_{\text{out}}^{\text{3D}}(\mathbf{r};E) = \frac{a_\perp}{\sqrt{\pi}} \int_0^\infty dk_\perp k_\perp e^{-a_\perp^2 k_\perp^2/2} J_0(k_\perp \sqrt{x^2+y^2}) \times \psi_{\text{out}}^{\text{1D}}\left(n,z;E-\frac{\hbar^2 k_\perp^2}{2m}\right). \tag{70}$$

C. Fermi gas

The wave function of a Fermi gas at $T=0$ is a Slater determinant of the product state of the wave functions of N atoms. The density profile and the current are just a sum of the currents and wave functions of the individual states of the atoms:

$$n_{\text{out}}(\mathbf{r};E) = \sum_n f(E_n)|\psi_{\text{out}}(n,\mathbf{r};E+E_n)|^2, \tag{71}$$

$$J(E) = \sum_n f(E_n) J_n(E+E_n), \tag{72}$$

where $f(E_n)$ is the Fermi distribution function. For a BCS superfluid gas with finite gap Δ the outcoupled density and current for each spin can be calculated using the BCS distribution function [56]

$$f_{\text{BCS}}(E_n) = 1 - \xi_n/\sqrt{\xi_n^2+\Delta^2}\tanh(\sqrt{\xi_n^2+\Delta^2}/2k_BT),$$

where $\xi_n = E_n - E_F$, E_F is the Fermi energy, and T the temperature of the system.

The current is shown in Fig. 7 for a spin-polarized normal gas. The 1D current in Eq. (69) has an energy spread on the order of the Fermi energy $E_F = N\hbar\omega_z$ due to the energy shifts

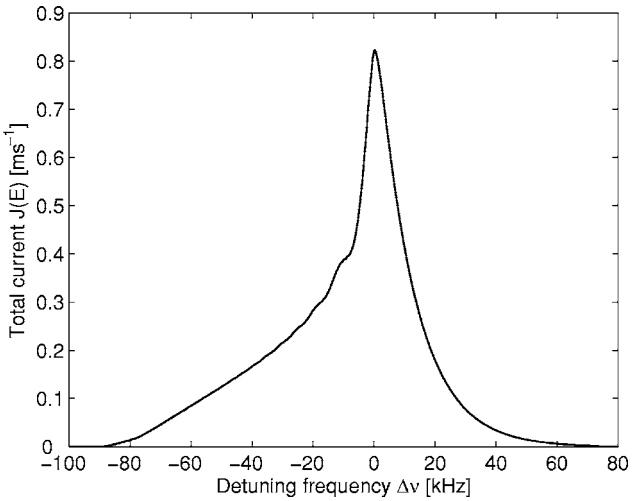

FIG. 7. Total 3D current for a quasi-1D Fermi gas [Eq. (72)] as a function of the detuning frequency $\Delta\nu = E/h$. Parameters: $N=70$ spin-polarized atoms, $\omega_z = 2\pi\times 1.2$ kHz, $\omega_\perp = 2\pi\times 120$ kHz, $E_F/h = 84$ kHz, $T=0$, $\gamma/h = 100$ Hz, and $m_{\text{K}} = 40$ u.

of the contributions of different modes. The convolution with the transverse direction results in an even wider spread of the total current, which is caused by the tight confinement in the transverse direction, as explained in Sec. V. It was predicted in [24] and demonstrated experimentally [26,54] that superfluidity in a Fermi gas leads to an energy shift in the outcoupled current when a rf (or laser) field transfers atoms from one of the paired hyperfine states to another hyperfine state. The shift originates in the additional energy needed to outcouple the atoms that are forming Cooper pairs. In the BCS regime considered here the gap cannot exceed a small percentage of the Fermi energy. Such values would not create an appreciable shift in the current in Fig. 7. However, in a strongly interacting fermionic superfluid [50–53] the gap can reach values of the order of $0.2E_F$ [26,54], which would lead to an experimentally detectable shift in the current in Fig. 7.

The one-particle correlation of the BEC was measured experimentally by outcoupling particles from the BEC with two different radio frequencies [10]. An equivalent process in a Fermi gas would lead to a density profile of the form

$$n(\mathbf{r},t;\nu_1,\nu_2) = \sum_n f(E_n)|\psi_{\text{out}}(n,\mathbf{r};h\nu_1+E_n)e^{ih\nu_1 t} + \psi_{\text{out}}(n,\mathbf{r};h\nu_2+E_n)e^{ih\nu_2 t}|^2. \tag{73}$$

As demonstrated in Fig. 8, the density profile at the center of the beam shows oscillations. For a Fermi gas, the oscillations are not related to superfluidity as in a BEC [see Eq. (33) and [10]]. In 1D, the density profile (73) is a sum of oscillatory functions in $E+Fz$ [see Eq. (66)]. Each of the terms in the sum is shifted by $\hbar\omega_z$, but because $E_F \ll Fz$, the period of oscillation is effectively the same. The 3D density profile (70) is a convolution of the 1D density function with the energy of the transverse directions that would result in oscillations on the scale $E+Fz$. Each term of the sum will contribute again by shifting the rescaled energy, and as long as

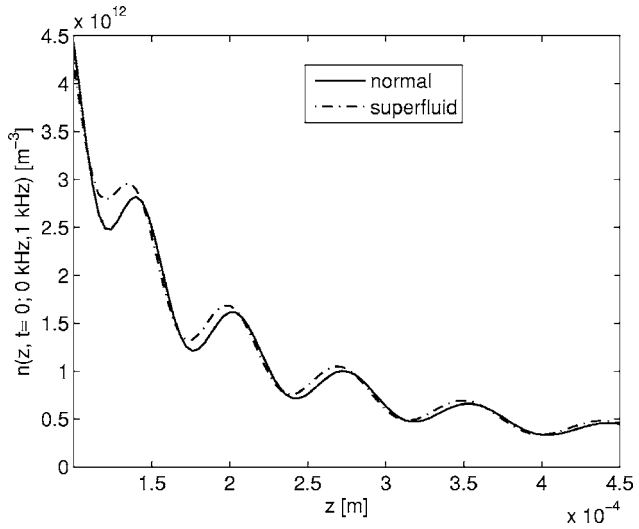

FIG. 8. Density profile of the fermionic beam outcoupled with two different radio frequencies $|E_{\mathrm{grav}}-E_{\mathrm{trap}}|/h$ and 1 kHz+$(E_{\mathrm{grav}}+E_{\mathrm{trap}})/h$. We show the density profile [Eq. (73)] at the center of the beam for a Fermi gas with $N=70$, $\omega_z=2\pi\times 1.2$ kHz, $\omega_\perp=2\pi\times 120$ kHz, and pairing gap $\Delta=3.36$ kHz, $\gamma/h=100$ Hz, and $m_{\mathrm{K}}=40$ u.

$E_F \ll Fz$, all of them will have effectively the same period of oscillation. As expected, the one-particle correlation function does not show any effect of the superfluidity. The gap energy shift transforms into a shift $\delta z=\Delta/F$ (see Fig. 8), which only leads to a time shift in the density profiles. Fermionic superfluidity relies on the formation of atomic pairs, and therefore one expects to see some effect of superfluidity only in the two-particle correlation function [57].

VII. SUMMARY AND OUTLOOK

A quantum-mechanical theory of the atom laser based on propagator techniques has been presented and contrasted with various approximation schemes. The analysis of the current and outcoupled beam leads to a distinction between small and big condensates. The experimentally observed structure and substructure [18,19] of the transverse beam profile has been obtained using the T-matrix formalism, which includes the effect of interactions.

The effect of a nonisotropic geometry of the trap has been analyzed, and a simple way to convolute the propagation along the gravitational and transverse direction has been determined. We have extended the formalism to calculate the current and outcoupled beam from excited modes. We have applied it to calculate the current and beam profile for a quasi-1D Fermi gas. We have shown that the interference pattern of atoms outcoupled with two different radio frequencies show oscillations that are not related to superfluidity as in the case of a Bose gas. The effect of fermionic superfluidity in the current and outcoupled beam has been discussed.

ACKNOWLEDGMENTS

We appreciate helpful discussions with C. Bracher, M. Kleber, and P. Kramer. This work is supported by the Deutsche Forschungsgemeinschaft [Grant No. KR 2889 (Emmy Noether Program)], by the EPSRC through Project No. EP/C51933/1 and the ESF (BEC2000+). T.K. would like to thank M. Moshinky for the invitation and hospitality at UNAM during the completion of this work.

APPENDIX: RECURSION RELATIONS FOR THE CURRENT AND BEAM DENSITY FROM THE EXCITED MODES OF A TRAP

We derive Eq. (67) for the outcoupled wave function from an excited state in a one-dimensional harmonic trap. The generating function of the Hermite polynomials reads

$$H_n\left(\frac{z}{a}\right)=\left[\frac{\partial^n}{\partial t^n}\exp(-t^2+2tz/a)\right]_{t=0}. \tag{A1}$$

Inserting it into Eq. (66) leads to

$$\begin{aligned}\psi_{\mathrm{out}}^{\mathrm{1D}}(n,z,E)&=\gamma\int dz' G_{\mathrm{grav}}^{\mathrm{1D}}(z,z',E)\psi_n(z')\\&=\gamma\frac{1}{\sqrt{2^n n! a\sqrt{\pi}}}\int dz' G(z,z',E)H_n\left(\frac{z'}{a}\right)e^{-z'^2/2a^2}\\&=\gamma\frac{1}{\sqrt{2^n n!}}\left[\frac{\partial^n}{\partial t^n}e^{-t^2}\frac{\int dz' G(z,z',E)e^{-z'^2/2a^2+2tz'/a}}{\sqrt{a}\pi^{1/4}}\right]_{t=0}.\end{aligned} \tag{A2}$$

Introducing a new variable $z''=z'+2ta$ and using the translation law for the Green function [14], Eq. (33), yields

$$\begin{aligned}\psi_{\mathrm{out}}^{\mathrm{1D}}(n,z,E)&=\frac{\gamma}{\sqrt{2^n n!}}\\&\times\left[\frac{\partial^n}{\partial t^n}e^{-t^2+2t^2}\frac{\int dz'' G(z,z''+2ta,E)e^{-z''^2/2a^2}}{\sqrt{a}\pi^{1/4}}\right]_{t=0}\\&=\frac{\gamma}{\sqrt{2^n n!}}\left[\frac{\partial^n}{\partial t^n}e^{t^2}\frac{\int dz'' G(z-2ta,z'',E+2taF)e^{-z''^2/2a^2}}{\sqrt{a}\pi^{1/4}}\right]_{t=0}.\end{aligned} \tag{A3}$$

The z'' integration in the last expression yields the known outgoing wave function for $n=0$,

$$\begin{aligned}\psi_{\mathrm{out}}^{\mathrm{1D}}(n,z,E)&=\frac{\gamma}{\sqrt{2^n n!}}\left[\frac{\partial^n}{\partial t^n}e^{t^2}\psi_{\mathrm{out}}^{\mathrm{1D}}(0,z-2ta,E+2ta)\right]_{t=0}\\&=-\frac{\gamma}{\sqrt{2^n n!}}4\sqrt{2}\pi^{5/4}\sqrt{F\alpha\beta^3}e^{-8\alpha^6/3+2\alpha^2\tilde{\epsilon}}\mathrm{Ci}(\tilde{\epsilon}-2\tilde{\xi})\\&\times\left[\frac{\partial^n}{\partial t^n}e^{t^2-8\alpha^3 t}\mathrm{Ai}(\tilde{\epsilon}-4\alpha t)\right]_{t=0}=B(n,z,E)\end{aligned}$$

$$\times K(n,2,-8\alpha^3,-2\beta E+4\alpha^4,-4\alpha)]. \quad \text{(A4)}$$

Here, we separated the factors in front of the square brackets from the derivatives and used the $K(\cdots)$ notation of Ref. [55], Eq. (13):

$$K(n,\alpha_L,\alpha_L',\gamma_L,\delta_L)=\left[\frac{\partial^n}{\partial t^n}e^{\alpha_L t^2/2+\alpha_L' t}\mathrm{Ai}(\gamma_L+\delta_L t)\right]_{t=0}. \quad \text{(A5)}$$

The expressions $K(n)$ are readily calculated using a recursion relation derived in [55], which we show here for completeness. One can define

$$K'(n,\alpha_L,\alpha_L',\gamma_L,\delta_L)=\left[\frac{\partial^n}{\partial t^n}e^{\alpha_L t^2/2+\alpha_L' t}\mathrm{Ai}'(\gamma_L+\delta_L t)\right]_{t=0} \quad \text{(A6)}$$

and simultaneously calculate $K(n)$ and $K'(n)$:

$$K(0)=\mathrm{Ai}(\gamma_L),\quad K(1)=\alpha_L' K(0)+\delta_L K_L'(0),$$

$$K'(0)=\mathrm{Ai}'(\gamma_L),\quad K'(1)=\alpha_L' K'(0)+\delta_L\gamma_L K(0),$$

$$K(n)=\alpha_L' K(n-1)+\alpha_L(n-1)K(n-2)+\delta_L K'(n-1),$$

$$K'(n)=\alpha_L' K'(n-1)+\alpha_L(n-1)K'(n-2)+\delta_L\gamma_L K(n-1)+\delta_L^2(n-1)K(n-2). \quad \text{(A7)}$$

As pointed out in [55] the recursion method is unstable for $|\delta_L|<1/2$ and for large γ_L. This means that we cannot use this method to calculate the current and outcoupled beam profile for small trapping frequencies or a large number of atoms. For small trapping frequencies, one could use the reflection approximation, Eq. (32).

[1] S. Choi and N. P. Bigelow, J. Opt. B: Quantum Semiclassical Opt. **7**, S413 (2005).
[2] M.-O. Mewes, M. R. Andrews, D. M. Kurn, D. S. Durfee, C. G. Townsend, and W. Ketterle, Phys. Rev. Lett. **78**, 582 (1997).
[3] B. P. Anderson and M. A. Kasevich, Science **282**, 1686 (1998).
[4] G. Cennini, G. Ritt, C. Geckeler, and M. Weitz, Phys. Rev. Lett. **91**, 240408 (2003).
[5] T. Kramer and M. Moshinsky, J. Phys. A **38**, 5993 (2005).
[6] E. W. Hagley, L. Deng, M. Kozuma, J. Wen, K. Helmerson, S. L. Rolston, and W. D. Phillips, Science **283**, 1706 (1999).
[7] N. P. Robins, C. Figl, S. A. Haine, A. K. Morrison, M. Jeppesen, J. J. Hope, and J. D. Close, Phys. Rev. Lett. **96**, 140403 (2006).
[8] I. Bloch, T. W. Hänsch, and T. Esslinger, Phys. Rev. Lett. **82**, 3008 (1999).
[9] A. P. Chikkatur, Y. Shin, A. E. Leanhardt, D. Kielpinski, E. Tsikata, T. L. Gustavson, D. E. Pritchard, and W. Ketterle, Science **296**, 2193 (2002).
[10] I. Bloch, T. W. Hänsch, and T. Esslinger, Nature (London) **403**, 166 (2000).
[11] M. Köhl, T. W. Hänsch, and T. Esslinger, Phys. Rev. Lett. **87**, 160404 (2001).
[12] A. Öttl, S. Ritter, M. Köhl, and T. Esslinger, Phys. Rev. Lett. **95**, 090404 (2005).
[13] T. Kramer, C. Bracher, and M. Kleber, J. Phys. A **35**, 8361 (2002).
[14] C. Bracher, T. Kramer, and M. Kleber, Phys. Rev. A **67**, 043601 (2003).
[15] J. Schneider and A. Schenzle, Appl. Phys. B: Lasers Opt. **69**, 353 (1999).
[16] F. Gerbier, P. Bouyer, and A. Aspect, Phys. Rev. Lett. **86**, 4729 (2001); **93**, 059905(E) (2004).
[17] T. Busch, M. Köhl, T. Esslinger, and K. Mølmer, Phys. Rev. A **65**, 043615 (2002); **65**, 069902(E) (2002).
[18] M. Köhl, T. Busch, K. Mølmer, T. W. Hänsch, and T. Esslinger, Phys. Rev. A **72**, 063618 (2005).
[19] J.-F. Riou, W. Guerin, Y. L. Coq, M. Fauquembergue, P. Bouyer, V. Josse, and A. Aspect, Phys. Rev. Lett. **96**, 070404 (2006).
[20] T. Kramer, Ph.D. thesis, Technische Universität München, 2003; online: http://tumb1.biblio.tu-muenchen.de/publ/diss/ph/2003/kramer.html
[21] T. Kramer, in *Squeezed States and Uncertainty Relations* (Rinton Press, Princeton, 2003), pp. 210–217; online: http://arxiv.org/abs/quant-ph/0309134
[22] I. Halperin and L. Schwartz, *Introduction to the Theory of Distributions* (University of Toronto Press, Toronto, 1952).
[23] E. J. Heller, J. Chem. Phys. **68**, 2066 (1978).
[24] P. Törmä and P. Zoller, Phys. Rev. Lett. **85**, 487 (2000).
[25] G. M. Bruun, P. Törmä, M. Rodríguez, and P. Zoller, Phys. Rev. A **64**, 033609 (2001).
[26] J. Kinnunen, M. Rodríguez, and P. Törmä, Science **305**, 1131 (2004).
[27] F. I. Dalidchik and V. Z. Slonim, Zh. Eksp. Teor. Fiz. **70**, 47 (1976) [Sov. Phys. JETP **43**, 25 (1976)].
[28] Y. L. Li, C. H. Liu, and S. J. Franke, J. Acoust. Soc. Am. **87**, 2285 (1990).
[29] B. Gottlieb, M. Kleber, and J. Krause, Z. Phys. A **339**, 201 (1991).
[30] The detuning is usually defined as $\Delta\nu_{\mathrm{expt}}=|\nu|-|E_{\mathrm{grav}}-E_{\mathrm{trap}}|$ [8]. For the usual states of ^{87}Rb, $(E_{\mathrm{grav}}-E_{\mathrm{trap}})<0$, which makes $\Delta\nu=E/h=-\Delta\nu_{\mathrm{expt}}$ using our definition of E, Eq. (13). Note that for $(E_{\mathrm{grav}}-E_{\mathrm{trap}})>0$ our definition of detuning agrees with $\Delta\nu_{\mathrm{expt}}$.
[31] T. Schumm, S. Hofferberth, L. M. Andersson, S. Wildermuth, S. Groth, I. Bar-Joseph, J. Schmiedmayer, and P. Kruger, Nat. Phys. **1**, 57 (2005).
[32] G. Herzberg, *Molecular Spectra and Molecular Structure* (Van Nostrand, Princeton, 1950).
[33] B. Hüpper and B. Eckhardt, Phys. Rev. A **57**, 1536 (1998).
[34] Y. Japha and B. Segev, Phys. Rev. A **65**, 063411 (2002).
[35] F. Dalfovo, S. Giorgini, L. P. Pitaevskii, and S. Stringari, Rev.

Mod. Phys. **71**, 463 (1999).
[36] G. Baym and C. J. Pethick, Phys. Rev. Lett. **76**, 6 (1996).
[37] C. J. Pethick and H. Smith, *Bose-Einstein Condensation in Dilute Gases* (Cambridge University Press, Cambridge, England, 2002).
[38] B. Donner, M. Kleber, C. Bracher, and H. J. Kreuzer, Am. J. Phys. **73**, 690 (2005).
[39] G. Möllenstedt and C. Jönsson, Z. Phys. **155**, 472 (1959).
[40] C. Blondel, C. Delsart, and F. Dulieu, Phys. Rev. Lett. **77**, 3755 (1996).
[41] C. Blondel, C. Delsart, F. Dulieu, and C. Valli, Eur. Phys. J. D **5**, 207 (1999).
[42] G. Galilei, *Discorsi e dimostrazioni matematiche intorno a due nuove scienze attenenti alla mecanica & i movimenti locali* (Leiden, 1638) [*Dialogues concerning Two New Sciences*, translated by Henry Crew and Alfonso Di Salvio, (Prometheus, Buffalo, NY, 1991)].
[43] M. Berry and K. W. Mount, Rep. Prog. Phys. **35**, 315 (1972).
[44] Y. N. Demkov, V. D. Kondratovich, and V. N. Ostrovskii, Pis'ma Zh. Eksp. Teor. Fiz. **34**, 425 (1981) [JETP Lett. **34**, 403 (1982)].
[45] C. Bracher, W. Becker, S. A. Gurvitz, M. Kleber, and M. S. Marinov, Am. J. Phys. **66**, 38 (1998).
[46] A. Görlitz *et al.*, Phys. Rev. Lett. **87**, 130402 (2001).
[47] F. Schreck, L. Khaykovich, K. L. Corwin, G. Ferrari, T. Bourdel, J. Cubizolles, and C. Salomon, Phys. Rev. Lett. **87**, 080403 (2001).
[48] M. Greiner, I. Bloch, O. Mandel, T. W. Hänsch, and T. Esslinger, Phys. Rev. Lett. **87**, 160405 (2001).
[49] B. DeMarco and D. S. Jin, Science **285**, 1703 (1999).
[50] C. A. Regal, M. Greiner, and D. S. Jin, Phys. Rev. Lett. **92**, 040403 (2004).
[51] M. W. Zwierlein, J. R. Abo-Shaeer, A. Schirotzek, C. H. Schunck, and W. Ketterle, Nature (London) **435**, 1047 (2005).
[52] T. Bourdel, L. Khaykovich, J. Cubizolles, J. Zhang, F. Chevy, M. Teichmann, L. Tarruell, S. J. J. M. F. Kokkelmans, and C. Salomon, Phys. Rev. Lett. **93**, 050401 (2004).
[53] G. B. Partridge, K. E. Strecker, R. I. Kamar, M. W. Jack, and R. G. Hulet, Phys. Rev. Lett. **95**, 020404 (2005).
[54] C. Chin, M. Bartenstein, A. Altmeyer, S. Riedl, S. Jochim, J. H. Denschlag, and R. Grimm, Science **305**, 1128 (2004).
[55] J. Lermé, Chem. Phys. **145**, 67 (1990).
[56] M. Tinkham, *Introduction to Superconductivity* (McGraw-Hill, New York, 1996).
[57] M. Greiner, C. A. Regal, J. T. Stewart, and D. S. Jin, Phys. Rev. Lett. **94**, 110401 (2005).